Magnetic signatures of serpentinization at ophiolite complexes

D. Bonnemains, J. Carlut, J. Escartin, C. Mével, M. Andreani, B. Debret

AGU PUBLICATIONS

Geochemistry, Geophysics, Geosystems

RESEARCH ARTICLE
10.1002/2016GC006321

Magnetic signatures of serpentinization at ophiolite complexes

D. Bonnemains[1], J. Carlut[1], J. Escartín[1], C. Mével[1], M. Andreani[2], and B. Debret[3]

[1]Institut de Physique du Globe de Paris, Sorbonne Paris Cité, Univ. Paris Diderot, UMR 7154, CNRS, Paris, France, [2]Univ. Lyon, Université Lyon 1, ENS de Lyon, UMR 5276 LGL-TPE, CNRS, Villeurbanne, France, [3]Department of Earth Sciences, Durham University, Durham, UK

Key Points:
- Ophiolite serpentinites display contrasted magnetic properties regardless of serpentinization degree
- Magnetic properties of serpentinites from ophiolites can be used as a proxy to differentiate their serpentinization setting (on or off axis)
- Both on-axis and off-axis serpentinization are able to produce significant hydrogen release

Supporting Information:
- Supporting Information S1
- Supporting Information S2

Correspondence to:
D. Bonnemains,
diane.bonnemains@gmail.com

Citation:
Bonnemains, D., J. Carlut, J. Escartín, C. Mével, M. Andreani, and B. Debret (2016), Magnetic signatures of serpentinization at ophiolite complexes, *Geochem. Geophys. Geosyst.*, *17*, 2969–2986, doi:10.1002/2016GC006321.

Received 24 FEB 2016
Accepted 28 JUN 2016
Accepted article online 1 JUL 2016
Published online 5 AUG 2016

Abstract We compare magnetic properties of 58 variably serpentinized peridotites from three ophiolite complexes (Pindos, Greece; Oman; Chenaillet, France) and the mid-Atlantic Ridge near the Kane fracture zone (MARK). The Pindos and Oman sites show low susceptibility and remanence ($K < 0.02$ SI; $M_s < 0.4$ Am^2/kg), while the Chenaillet and MARK sites show instead high susceptibility and remanence (K up to 0.15 SI; M_s up to 6 Am^2/kg), regardless of serpentinization degree. Petrographic observations confirm that Pindos and Oman samples contain serpentine with very little magnetite, while Chenaillet and MARK samples display abundant magnetite in serpentine mesh cells. Bulk rock analyses show similar amounts of ferric iron at a given serpentinization degree, suggesting that iron is oxidized during the serpentinization reaction in both cases, but that its distribution among phases differs. Microprobe analyses show iron-rich serpentine minerals (5–7 wt % FeO) in low-susceptibility samples, while iron-poor serpentine minerals (2–4 wt % FeO) occur in high susceptibility samples. The contrasted magnetic properties between the two groups of sites thus reflect different iron partitioning during serpentinization, that must be related to distinct conditions at which the serpentinization reaction takes place. We propose that magnetic properties of ophiolitic serpentinites can be used as a proxy to differentiate between high temperature serpentinization ($>\sim$250–300°C) occurring at the axis (i.e., Chenaillet, similar to serpentinites from magmatically poor mid-ocean ridges), from lower temperature serpentinization ($<\sim$200–250°C), likely occurring off axis and possibly during obduction (i.e., Pindos and Oman). At both settings, serpentinization can result in significant hydrogen release.

1. Introduction

Serpentinization is a major process affecting peridotites when they react with hydrous fluids. Serpentinization occurs dominantly at temperatures below ~400°C through a multistage process [e.g., review in *Mével*, 2003; *Bach et al*., 2006; *Früh-Green et al*., 2004; *McCollom and Bach*, 2009; *Klein et al*., 2009]. This reaction significantly modifies the physical and mechanical properties of the lithosphere [e.g., *Christensen*, 1978; *Escartín et al*., 2001]. Peridotites from the oceanic lithosphere may be serpentinized in different geodynamic settings, from the ridge axis to both passive and active continental margins. The serpentinization process leads to the oxidation of ferrous mantle minerals into Fe^{3+}-rich serpentines and magnetite [e.g., *Andreani et al*., 2013]. Based on existing data from oceanic serpentinites, *Klein et al*. [2014] suggested that the abundance of magnetite formed during serpentinization is controlled by reaction temperature, confirming previous experiments and thermodynamic models [*Seyfried et al*., 2007; *Klein et al*., 2009; *Malvoisin et al*., 2012a, 2012b; *Klein et al*., 2013]. As the overall thermal regime of the lithosphere depends on the geodynamic context, *Klein et al*. [2014] suggested that serpentinization at mid-ocean ridges, where abundant magnetite is produced, occurs at high temperatures ($>\sim$200°C), while serpentinization at passive margins or fore arcs producing little or no magnetite, occurs at low temperatures ($<\sim$200°C).

Ophiolite complexes are remnants of the oceanic lithosphere formed either at mid-oceanic ridges or in back arc environments, subsequently incorporated into mountain belts at convergent margins and exposed on-land. Mantle peridotites from these complexes show a wide range of serpentinization degrees, but a limited amount of data on their magnetic properties are available [*Lienert and Wasilewski*, 1979; *Toft et al*., 1990; *Maffione et al*., 2014]. Because ophiolites have experienced a complex tectonic history until their final emplacement, it is often unclear when serpentinization occurred.

In this paper, we investigate the magnetic properties of variably serpentinized peridotites from several ophiolites (Pindos in Greece, Oman, and Chenaillet in France) and compare these to serpentinized samples from near-axis oceanic lithosphere (Kane area, mid-Atlantic Ridge) and with published data from other oceanic sites. We relate these magnetic properties to microtextures and geochemistry. We discuss our new data and observations in terms of temperature of serpentinization and geodynamic setting where the main phase of hydration occurred.

2. Sample Selection

We have selected variably serpentinized peridotites from a set of ophiolite massifs, whose former oceanic lithosphere had different structure and geodynamic evolutions. In addition, we have selected a few samples drilled near-axis in the MARK area along the mid-Atlantic Ridge, complementing a prior magnetic study of *Oufi et al*. [2002] with additional magnetic measurements and geochemical analyses.

2.1. Pindos

The Pindos ophiolite (Greece) is one of several ophiolites along the Hellenic margin that likely correspond to an originally magmatic, layered oceanic crust, with remnants of a clear dyke complex and an overlying lava section [e.g., *Rassios and Dilek*, 2009]. The crustal thickness varies between 3 and ~5 km [e.g., *Robertson*, 2002; *Saccani and Photiades*, 2004; *Rassios and Moores*, 2006]. This crust formed in the Jurassic Tethyan basin, and was subsequently obducted [see *Robertson*, 2002; *Rassios and Dilek*, 2009, and references therein]. Twenty-two peridotites varying from fresh to highly serpentinized were collected from this ophiolite. This suite of samples is used here to investigate the dependence of magnetic properties on serpentinization degree. This set of samples is also more complete than a similar Pindos suite used by *Schmitt et al*. [2007] to study the links between serpentinization, magnetic susceptibility, and seismic anisotropy.

2.2. Oman

For comparison with the Pindos suite, we selected 15 representative peridotites samples from several massifs throughout the Oman ophiolite, with serpentinization degrees ranging from moderately to highly serpentinized. Precise location and petrographic description of the samples can be found elsewhere [*Monnier et al*., 2006]. This ophiolite displays one of the best-preserved, continuous magmatic crustal sections, with a thickness of more than 5 km and a well-developed dyke complex [e.g., *Christensen and Smewing*, 1981; *Nicolas et al*., 1996]. Owing to the crustal continuity and preservation, its composition and structure has been adopted as a model for the oceanic crust formed along fast-spreading ridges [e.g., *Christensen and Smewing*, 1981; *Nicolas et al*., 2009].

2.3. The Chenaillet Ophiolite (Montgenèvre, Western Alps)

We have selected seven samples from the Chenaillet ophiolite (Montgenèvre, Western Alps, France) with high serpentinization degrees, as weakly serpentinized samples are not available due to pervasive serpentinization of this ophiolite. This Thetyan ophiolite differs from Pindos and Oman in that it corresponds to an originally heterogeneous oceanic crust composed of gabbro and peridotite, instead of a continuous and layered magmatic oceanic crust. The exposure of serpentinized peridotites at the seafloor at the ridge axis is documented and is possibly associated with detachment faulting [e.g., *Lemoine et al*., 1987; *Lagabrielle and Polino*, 1988; *Manatschal et al*., 2011]. Two of the samples used here (ICh02 and BCh10) are also reported in *Debret et al*. [2014], where the amount of magnetite is discussed in relation with serpentine recrystallization during devolatilization.

2.4. Mid-Atlantic Ridge South of Kane: MARK Area

We have analyzed 14 samples from ODP Leg 152, hole 920, all highly serpentinized peridotites. This site was drilled along a major rift-bounding fault that exposes mantle, gabbro, and other mafic rocks of a compositionally heterogeneous lithosphere [e.g., *Karson et al*., 1987; *Mével et al*., 1991; *Cannat*, 1993; *Cannat et al*., 1995]. At this site, serpentinization is related to tectonic uplift and exhumation near axis [e.g., *Andreani et al*., 2007], and the overall crustal structure and composition may be comparable to that proposed for the Chenaillet ophiolite (see above). Our results expand existing magnetic data sets for this site [*Cannat et al*., 1995; *Oufi et al*., 2002].

3. Analytical Methods

3.1. Density Measurements and Serpentinization Degree

Sample density and porosity were measured using the triple weighing method [e.g., *Dullien*, 1992] with a Sartorius Density Determination Kit. Samples weighting a few grams were first placed inside an oven at 60°C during 24 h and weighted (m_{dry}) . This was followed by 24 h in a vacuum desiccator at −1 bar, and subsequently immersed 24 h in water. The water-saturated weight in air (m_{sat}) was then measured, followed by the immersed weight (m_{imm}). Grain density (ρ_g) is then calculated using

$$\rho_g = \frac{m_{dry}}{(1-\varphi).(m_{sat}-m_{imm}) \ . \ \rho_w},$$

where ρ_w is the density of water, and ϕ is the porosity expressed as

$$\phi = \frac{m_{sat}-m_{dry}}{m_{sat}-m_{imm}}.$$

Multiple measurements were performed for each sample, which allowed us to evaluate the uncertainty in density measurements at $\sim 10^{-2}$ g/cm^3.

Serpentinization degree (S) is calculated assuming that the samples only contain olivine and serpentinite, with densities of 3.300 and 2.515 g/cm^3, respectively, according to the empirical relation of *Miller and Christensen* [1997]: $\rho_g = 3.30 - 0.785 \times S$. This method does not take into account the formation of secondary magnetite and therefore the density-based serpentinization degree may slightly underestimate the actual serpentinization degree. For example, a serpentinite (S = 100%) containing a maximum amount of 5% magnetite of density 5.2 g/cm^3, would have a density of ∼2.65 g/cm^3. The density-derived serpentinization degree would thus be 83% instead of the actual 100%, and a similar bias is expected if other minor phases denser than serpentinite are present (e.g., spinel and pyroxenes). Density-derived values of S given in Table 1 are thus an objective measure even if they may slightly underestimate the actual serpentinization degree.

3.2. Magnetic Measurements

Magnetic susceptibility at room temperature was measured on 2–7 minicores (∼200 mg) per sample with a Kappabridge instrument (KLY-3) at Institut de Physique du Globe de Paris (IPGP, France). Magnetic hysteresis parameters were acquired on the same minicores using a Vibrating Sample Magnetometer (VSM, Micro-Mag 3900, at IPGP) at ambient conditions. A field of 500 mT was sufficient to reach magnetic saturation in all samples. Classical hysteresis parameters (paramagnetic slope, saturation magnetization M_s, remanent saturation magnetization M_{rs}, and coercive forces H_{cr} and H_c) have been determined during this experiment (see a representative example of hysteresis loop in supporting information Figure S1). Low field susceptibility has been monitored using a KLY-3 equipped with a CS-3 on ∼100 mg powdered samples during heating and cooling up to 620°C with an increment of 8°C/min. Argon was injected during the measurements to avoid oxidation reactions during heating.

Field cooled (FC) and zero field cooled (ZFC) remanence measurements were carried out on powder samples weighting a few mg using a Quantum Designs™ superconducting device Magnetic Properties Measurement System (SQUID MPMS) at IPGP. The moment was measured as the sample was progressively warmed from 10 to 300 K in a 0 T field. ZFC data were obtained after the samples were previously cooled from 300 to 10 K in a 0 T field, at 10 K a 2.5 T field is rapidly applied. FC data were obtained after cooling the samples in a 2.5 T field, and warming them to 300 K in 5 K steps.

3.3. Mineralogical and Geochemical Studies

Observation and semiquantitative chemical data were collected on thin sections using an optical microscope and two field emission scanning electronic microscopes (Fe-SEM, Zeiss Sigma and Zeiss Auriga) equipped with EDS detectors (Oxford instrument) at École Normale Supérieure de Paris (ENS Paris) and at IPGP. Quantitative mineral analyses were obtained using an Electron Probe MicroAnalyzer EPMA (CAMECA SX-FIVE) at CAMPARIS (UPMC, Paris). Serpentine polymorphs were identified by Raman spectroscopy using a Renishaw InVia with a green argon laser (20 mW, 514 nm) at ENS Paris. Whole rock major element concentrations were determined by Inductively Coupled Plasma Optical Emission Spectrometry (ICP-OES) at the SARM-CRPG (Nancy, France) after fusion with $LiBO_2$ and dissolution with HNO_3. Separate analyses of whole

Table 1. Porosity, Grain Density, and Magnetic Properties of Serpentinized Peridotites[a] at Pindos, Oman, Chenaillet, and MARK

Site	Sample	ϕ %	d (g/cm^3)	S (%)	N	K (SI)	Km (m^3/kg)	M_s (Am^2/kg)	M_{rs} (Am^2/kg)	H_c (mT)	H_{cr} (mT)	Mt (%)	χ_{HF} (Am^2/T kg)
Pindos	P01-1[b]	0.3	3.261	5	3	7.01E-04	2.15E-07	0.01	0.00	14.74	29.95	0.01	0.13
	P01-2[b]	0.0	3.263	5	3	9.43E-04	2.89E-07	0.03	0.01	16.62	24.98	0.03	0.14
	P03-1[b]	0.3	3.217	11	5	2.91E-03	9.05E-07	0.10	0.03	20.98	33.57	0.11	0.18
	P03-2[b]	0.3	3.146	20	3	2.95E-03	9.36E-07	0.09	0.02	19.03	29.99	0.10	0.16
	P03-3[b]	0.2	3.100	25	3	2.01E-03	6.48E-07	0.06	0.02	15.61	25.91	0.07	0.14
	P04-1[b]	0.5	2.849	57	3	2.89E-03	1.02E-06	0.14	0.02	16.37	32.76	0.15	0.14
	P04-2[b]	0.6	2.858	56	3	1.64E-03	5.74E-07	0.06	0.01	21.55	41.33	0.06	0.15
	P05-1[b]	0.3	2.705	76	7	2.29E-03	8.47E-07	0.10	0.03	20.99	37.11	0.11	0.17
	P05-2[b]	0.3	2.769	68	2	1.97E-03	7.11E-07	0.08	0.02	17.76	31.55	0.09	0.16
	P06-1[b]	0.1	3.043	33	3	1.74E-03	5.70E-07	0.06	0.02	23.05	39.84	0.06	0.17
	P06-2[b]	0.9	2.699	77	3	1.57E-03	5.83E-07	0.06	0.02	24.10	39.46	0.07	0.18
	P06-3[b]	0.8	2.733	72	3	3.11E-03	1.14E-06	0.15	0.06	22.90	31.71	0.16	0.18
	P08-1	0.4	2.981	41	3	3.86E-03	1.30E-06	0.15	0.04	18.08	27.76	0.16	0.26
	P08-2[b]	0.1	3.158	18	2	3.87E-03	1.23E-06	0.13	0.04	19.95	30.18	0.14	0.19
	P08-3[b]	0.6	3.045	33	2	4.07E-03	1.34E-06	0.16	0.06	21.82	31.47	0.17	0.20
	P10-1[b]	0.1	3.283	2	3	9.70E-04	2.95E-07	0.02	0.00	17.85	33.15	0.02	0.14
	P10-2[b]	0.2	3.313	0	3	6.96E-04	2.10E-07	0.01	0.00	20.52	38.69	0.01	0.14
	P11-1[b]	0.2	3.278	3	3	1.61E-03	4.91E-07	0.05	0.00	16.19	38.37	0.05	0.14
	P11-2[b]	0.2	3.299	0	3	2.14E-03	6.47E-07	0.07	0.01	12.29	35.09	0.07	0.16
	P12-1[b]	0.2	3.234	8	3	4.88E-04	1.51E-07	0.00	0.00	25.23	45.25	0.00	0.12
	P13-1[b]	0.4	2.626	86	5	4.26E-03	1.62E-06	0.18	0.03	15.47	35.98	0.19	0.27
	P13-2[b,c]	0.5	2.613	87	2	4.00E-03	1.53E-06	0.20	0.03	15.69	34.66	0.21	0.27
Oman													0.00
	MAN69[b]	0.7	2.720	74	3	5.83E-04	2.14E-07	0.01	0.00	20.87	34.74	0.02	0.10
	MAN72	0.8	2.903	51	3	5.46E-04	1.88E-07	0.01	0.00	19.64	35.92	0.01	0.11
	MAN77[b]	11.4	3.158	18	4	6.48E-03	2.05E-06	0.29	0.07	15.91	27.77	0.32	0.19
	MAN78[b]	0.7	2.826	60	3	5.38E-04	1.90E-07	0.01	0.00	27.49	44.53	0.01	0.12
	MAN79A	1.2	2.793	65	3	1.02E-03	3.64E-07	0.04	0.01	25.46	37.85	0.04	0.12
	MAN80	1.3	2.919	49	3	3.95E-03	1.35E-06	0.21	0.08	28.51	48.70	0.22	0.18
	MAN84[b]	1.0	2.764	68	3	5.08E-03	1.84E-06	0.26	0.08	16.07	24.51	0.29	0.17
	MAN97	0.5	2.840	59	3	7.11E-03	2.51E-06	0.35	0.11	20.13	27.09	0.38	0.22
	MAN98[b]	1.3	2.938	46	3	1.01E-03	3.44E-07	0.03	0.01	14.33	26.27	0.03	0.12
	MAN99	0.6	3.016	36	3	9.85E-04	3.27E-07	0.03	0.01	18.25	40.64	0.03	0.13
	MAN107	1.1	2.917	49	3	1.34E-03	4.61E-07	0.07	0.02	20.38	35.39	0.07	0.13
	MAN108	0.9	2.903	51	3	2.42E-03	8.34E-07	0.05	0.02	26.51	42.39	0.06	0.14
	MAN125[b]	0.7	3.034	34	2	2.71E-03	8.93E-07	0.10	0.04	19.36	26.62	0.11	0.15
	MAN149	0.6	2.841	58	3	7.78E-03	2.74E-06	0.39	0.09	15.21	26.73	0.42	0.21
	MAN152	1.0	2.979	41	3	2.46E-03	8.27E-07	0.11	0.04	23.67	35.02	0.12	0.15
Chenaillet													0.00
	ICh02[b,c]	2.7	2.693	77	5	1.42E-01	5.27E-05	6.11	1.19	9.30	14.99	6.64	1.32
	BCh10[b,c]	1.7	2.707	76	4	1.44E-01	5.31E-05	5.14	0.81	7.22	10.88	5.58	1.35
	BCh11[b]	1.2	2.684	78	6	1.08E-01	4.01E-05	4.59	0.63	7.86	13.57	4.99	0.55
	PR03-1[b]	2.2	2.664	81.0	4	7.88E-02	2.96E-05	3.65	0.84	12.81	18.53	3.97	0.33
	PR05-2	1.3	2.676	79.4	4	9.34E-02	3.49E-05	4.81	1.15	14.63	20.85	5.23	0.42
	PR06-1	2.2	2.695	77.1	4	5.37E-02	1.99E-05	2.72	0.61	14.86	23.76	2.95	0.28
	PR08-1	3.2	2.691	77.5	4	6.38E-02	2.37E-05	3.21	0.80	14.12	20.23	3.48	0.30
MARK													0.00
Hole 920B	3R1 pc3 41-47cm	4.7	2.640	84	2	8.70E-02	3.30E-05	3.92	0.74	8.92	14.43	4.26	1.39
	6R1 pc3 20-26cm[b,c]	5.8	2.660	82	2	3.69E-02	1.39E-05	1.63	0.34	12.50	21.97	1.78	0.78
	6R1 pc8 75-81cm	13.0	2.620	87	2	5.08E-02	1.94E-05	2.05	0.46	9.89	22.09	2.23	0.82
	7R1 pc4 78-83cm	3.2	2.660	82	2	4.57E-02	1.72E-05	1.89	0.42	13.76	21.64	2.06	0.76
	7R2 pc8 113-117cm	3.1	2.640	84	2	5.53E-02	2.09E-05	2.10	0.40	16.28	24.75	2.28	1.06
	8R1 pc14 109-115cm[b]	3.8	2.680	79	2	1.09E-01	4.07E-05	4.48	0.78	8.64	14.29	4.86	1.63
	12R2 pc6 147-150cm	5.1	2.630	85	2	8.11E-02	3.08E-05	3.07	0.48	12.39	34.80	3.34	1.43
	1W2W-12-17	0.9	2.650	83	2	3.59E-02	1.35E-05	1.52	0.40	13.41	18.77	1.65	0.65
Hole 920D	10R2 pc7 116-120cm[b]	5.8	2.650	83	2	1.19E-01	4.51E-05	4.69	0.89	9.99	15.39	5.10	1.88
	14R2 pc4 30-34cm	4.2	2.750	70	2	5.92E-02	2.15E-05	2.36	0.33	10.54	20.23	2.57	0.93
	14R2 pc7 91-94cm[b]	1.6	2.880	54	2	7.79E-02	2.70E-05	3.23	0.73	13.64	21.09	3.51	1.56
	16R6 pc10 66-69cm	8.5	2.680	79	2	8.65E-02	3.23E-05	3.62	0.57	11.97	23.70	3.93	1.56
	16R5 pc5 126-130cm[b]	12.3	2.610	88	3	6.23E-02	2.39E-05	2.56	0.61	13.59	20.21	2.78	1.21
	19R1 pc7 61-65cm[b]	5.5	2.630	85	2	1.54E-02	5.87E-06	0.67	0.14	11.11	26.14	0.73	0.28
	20R2 pc5 59-64cm	4.3	2.650	83	2	8.55E-02	3.23E-05	3.14	0.69	12.05	19.05	3.41	0.65

[a] φ, porosity; d, grain density; S, serpentinization degree after grain density; N, number of minicores; K, magnetic susceptibility; Km, mass magnetic susceptibility; M_s, saturation magnetization; M_{rs}, saturation remanent magnetization; H_c, coercive force; H_{cr}, remanent coercive force; Mt, magnetite content; χ_{HF}, absolute value of high-field slope correction.
[b] Samples for which thermomagnetic curves have been acquired.
[c] Samples for which low temperature remanence analyses have been performed.

rock FeO contents were also performed by titration with potassium dichromate after dissolution of the sample in a HF/H_2SO_4 mixture in order to calculate Fe^{3+}/Fe^{Tot} ratios.

Punctual measurements of iron redox state in serpentine minerals has been extracted from the preedge region of Fe *K*-edge XANES (X-ray absorption near-edge structure) spectra of serpentine. Fe *K*-edge XANES spectroscopic measurements were performed at the ID24 beamline of the ESRF (European Synchrotron Radiation Facility; Grenoble, France). The description of the experimental setup and data treatment are explained in *Andreani et al*. [2013]. The method is based on the previous works of *Muñoz et al*. [2006] and *Wilke et al*. [2001].

4. Results

4.1. Serpentinization Degree

The grain density measured for 58 samples ranges from 3.31 to 2.61 g/cm^3, thus encompassing fresh to fully serpentinized peridotites (Table 1). The Pindos sample suite shows the broadest range of serpentinization (0%–87%), while that of Oman samples is slightly more restricted (18%–74%). The samples from Chenaillet and MARK show instead medium to high degrees of serpentinization (76–81% and 57–88%, respectively).

4.2. Magnetic Properties

4.2.1 Curie Temperature

Thermomagnetic curves have been acquired for Pindos (on 21 samples), Oman (6), Chenaillet (4), and MARK (7) samples. All samples display a dominant ferromagnetic phase with a sharp decrease in susceptibility after 570°C (Figure 1). The inferred Curie point using the inflection method is between 575°C and 585°C, attesting that nearly stoichiometric magnetite is likely the dominant magnetic carrier in all samples. The Chenaillet and MARK samples show a reversible behavior, indicating that little or no mineralogical changes happen during heating (Figures 1a and 1b). Samples from Pindos and Oman show irreversible behavior instead, as final susceptibility is higher at the end of the temperature cycle (Figures 1c and 1d). The increase in magnetization during cooling suggests destabilization of an iron-bearing phase to magnetite during the experiment in the laboratory. In the Oman samples, a hump is commonly observed on heating starting around 130–150°C and decreasing around 400°C (Figure 1d). A similar behavior is reported in other serpentinized samples [*MacLeod et al*., 2011; *Horen et al*., 2014] that is attributed to the alteration of Cr-spinel to ferrichromite, suggesting a specific alteration of the Cr-spinels during laboratory heating in the Oman samples.

4.2.2. Low Temperature Remanence

Low temperature remanence analyses performed on four powder subsamples from Pindos, Chenaillet, and MARK, show in all cases a strong Verwey transition around 120–128 K indicative of magnetite, as observed on two representative samples in Figure 2. The 20 K field cooled magnetization is slightly larger or equal to the 20 K zero field cooled magnetization, which is characteristic of single-domain to pseudo-single-domain magnetite [*Brachfeld et al*., 2002; *Smirnov*, 2009].

4.2.3. Susceptibility and Saturation Magnetization

Magnetic susceptibilities (K) measured on the Pindos and Oman samples range from 4.9×10^{-4} to 7.8×10^{-3} SI (1.5×10^{-7} to 2.7×10^{-6} m^3/kg). In contrast, susceptibilities from the Chenaillet and MARK samples have values more than one order of magnitude higher, with K ranging from 1.5×10^{-2} to 1.4×10^{-1} SI (5.9×10^{-6} to 5.3×10^{-5} m^3/kg) (Table 1, Figure 3). Similarly, the saturation magnetization (M_s) also displays an order of magnitude difference between the Pindos and Oman samples relative to the Chenaillet and MARK ones (Table 1). The relation between K and M_s is nearly linear ($M_s = 41.85 \times K$ ($R = 0.98$), Figure 3), and in agreement with the trend proposed by *Oufi et al*. [2002] for abyssal samples ($M_s = 40.65 \times K$). The good linearity between K and M_s found in this study and in *Oufi et al*. [2002] attests that in the case of serpentinized samples the magnetite grain size variation, to which K is sensitive but not M_s, is moderate enough to use susceptibility as a good indicator of magnetite concentration.

Assuming that magnetite is the dominant magnetic phase in our samples as suggested by the Curie temperatures and the Verwey transitions, the magnetite content (Mt) can be calculated using the following equation [*O'Reilly*, 1984]:

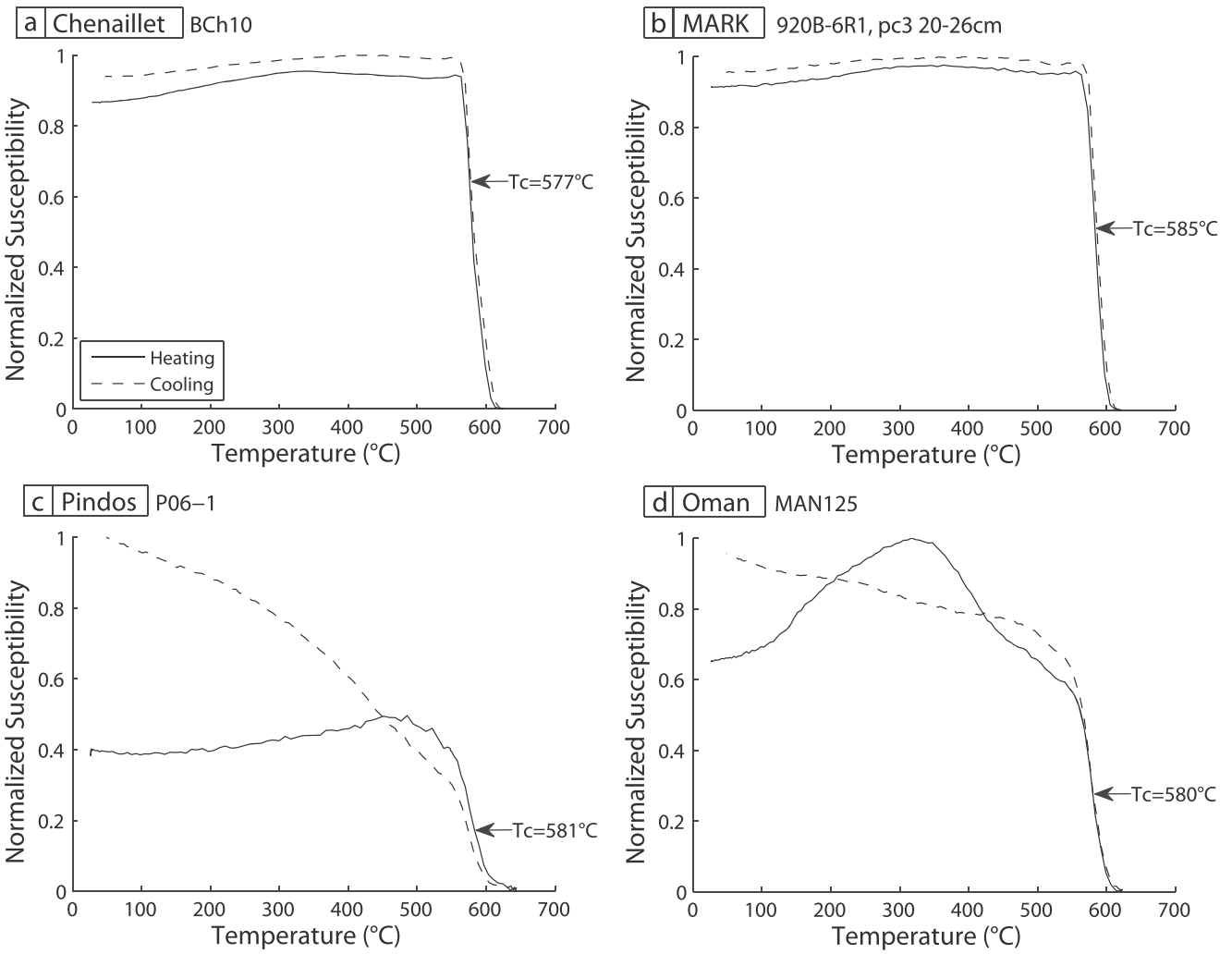

Figure 1. Examples of representative mass normalized thermomagnetic curves for (a) Chenaillet, (b) MARK, (c) Pindos, and (d) Oman. The Curie temperatures corresponding to the inflection point during the sharp decrease in susceptibility is given for each sample.

$$\text{Mt}\ (\%) = 100.\frac{Ms_{+sample}}{Ms_{+magnetite}},\ \text{with}\ M_{s\ magnetite} = 92\ \text{Am}^2/\text{kg}.$$

Magnetite contents for the Pindos and Oman samples show relatively homogeneous values, typically below 0.4%. In the case of the Chenaillet and MARK samples, magnetite content is very heterogeneous, with the higher values reaching up to 6.6%.

Magnetic susceptibility relative to grain density and serpentinization degree is represented in Figure 4a for a compilation of oceanic samples, including continental rifted margins, mid-ocean ridges and subduction zone fore arcs. Serpentinites from mid-ocean ridge environments (from the literature and this study for the MARK area) show a wide range of magnetic susceptibilities from ~0 to 0.13 SI. In contrast, serpentinites from continental margins and subduction areas systematically display low magnetic susceptibility, uncorrelated to the serpentinization degree, and with only a small overlap with mid-ocean ridge samples at very low magnetic susceptibilities ($K < 0.02$ SI). Figure 4b displays the susceptibility measured in the studied ophiolite samples in comparison with the different oceanic domains defined from the data compilation in Figure 4a. The Chenaillet samples overlap with the mid-ocean ridge domain, and reach high values of $K = 0.14$ SI. In contrast, the Pindos and Oman samples display low magnetic susceptibilities ($K < 0.01$ SI) that overlap with domain defined by samples from subduction zones and continental rifted margin. As

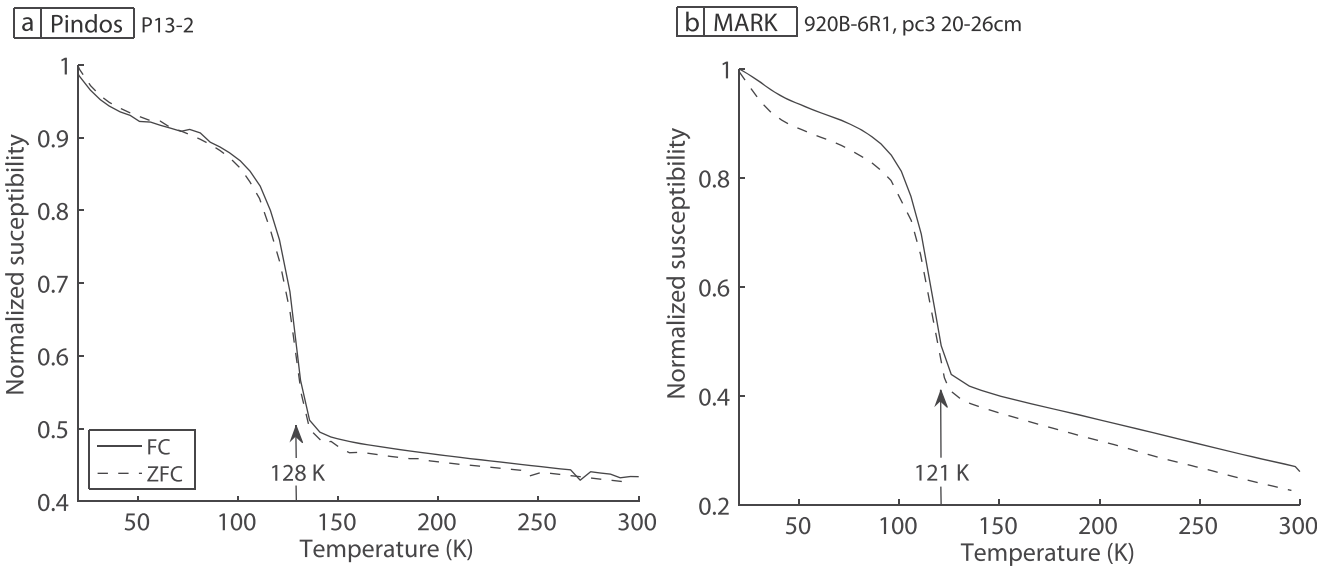

Figure 2. Representative low temperature remanence curves for (a) low-magnetite and (b) high-magnetite content samples (Pindos and MARK, respectively). Arrows indicate Verwey transition temperature for each sample. Abbreviations: FC, field cooled; ZFC, zero field cooled.

shown by the positive correlation between K and M_s (Figure 3), these differences in magnetic susceptibility can be directly related to magnetite content, being more abundant within the Chenaillet serpentinite samples than within the Oman and Pindos ones.

4.2.4. Magnetic Grain Size

The hysteresis parameters M_{rs}/M_s and H_{cr}/H_c are used to constrain the magnetic grain size distribution, based on theoretical mixing curves obtained for different magnetite grain morphologies (curves 1–3, Figure 5) of single-domain (SD) and multiple-domain (MD) grains [*Dunlop*, 2002a, 2002b]. SD percentage for the majority of samples ranges from 40% to 80%. Hence magnetite in all samples is relatively fine grained, judging by hysteresis values. Most Chenaillet and MARK samples lie slightly below the SD-MD mixing theoretical curves, a behavior already observed by *Dunlop* [2002b] for oceanic serpentinized peridotites, but that remains unexplained.

The M_{rs}/M_s ratio for each sample as a function of serpentinization represented in Figure 6 does not display any clear dependence, indicating that magnetite grain size is not correlated with serpentinization degree. In particular, the Chenaillet and MARK samples, that are highly serpentinized, display a large variability in M_{rs}/M_s, while the Pindos samples show a similar spread at both high and low degrees of serpentinization ($M_{rs}/M_s \sim 0.15$–0.4). This lack of correlation with degree of serpentinization is consistent with that reported for oceanic samples [*Oufi et al.*, 2002] and for experimental serpentinization products [*Malvoisin et al.*, 2012a] but contrasts with values for Mirdita ophiolite samples, which suggest a growth of MD magnetite with increasing serpentinization degree [*Maffione et al.*, 2014].

4.3. Mineral Assemblages and Geochemistry

To understand the magnetic properties of the studied samples, we have collected mineralogical and geochemical data. Optical (Figure 7) and SEM observations (Figure 8) show that serpentinite textures and mineral assemblages vary among the different localities. In the less serpentinized samples from Pindos, the olivine is crosscut by a network of serpentine-filled veins, whereas in fully serpentinized samples, the olivine is replaced by mesh textures (Figure 7a). The local degree of serpentinization can be very heterogeneous at the thin section scale, and orthopyroxene remains essentially fresh, regardless of serpentinization degree. Magnetite is present in very small amounts and is mainly observed in serpentine veins crossing mesh textures (Figure 7a), even in highly serpentinized rocks. Magnetite grains are small (<4 μm) with irregular grain shapes and boundaries (Figure 8a). In some samples, we observe orange patches within serpentinite veins and along their edges (red arrows in Figure 7a).

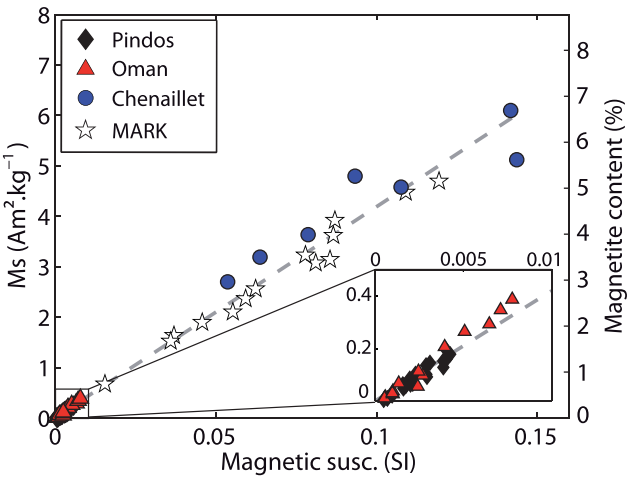

Figure 3. Saturation magnetization (M_s), and its equivalent magnetite content, and susceptibility (K) for all minicores from Pindos, Oman, Chenaillet, and MARK. The black dotted line represents the best fitting relation between M_s and K ($M_s = 41.85 \times K$, R = 0.98). Inset is a blowup to show the Pindos and Oman samples.

Textures and mineral assemblages of the Oman serpentinites are similar to those from the Pindos samples. The Oman samples display mesh texture without magnetite formed after alteration of olivine (Figure 7b), and orthopyroxenes display little to no alteration. Small-sized magnetite grains of irregular shapes crystallize along veins that are few hundred micrometers wide (Figure 8b). Orange to brown patches are also locally observed on the border of serpentine-filled veins (red arrows in Figure 7b).

In contrast, the highly serpentinized Chenaillet samples display mesh-textures with abundant magnetite along the mesh boundaries (Figure 7c). Orthopyroxenes are fully serpentinized forming bastites. The magnetite grains in the mesh can reach sizes of a few micrometers, but they are typically $<$10 μm, and display well-defined euhedral shapes (Figure 8c).

The oceanic samples from the Chenaillet are very similar to those from MARK, as they all display typical mesh textures formed after olivine and underlined by abundant magnetite surrounding the mesh cells (Figure 7d), and orthopyroxenes are also largely altered to bastite. The shape and size of magnetite grains from the mesh rims (Figure 8d) are similar to those from Chenaillet samples (Figure 8c).

Using Raman spectroscopy, we have determined that the dominant serpentine type in our samples is lizardite (Figure 9a). Chrysotile occurs only in late veins from Chenaillet and MARK samples, while we identified

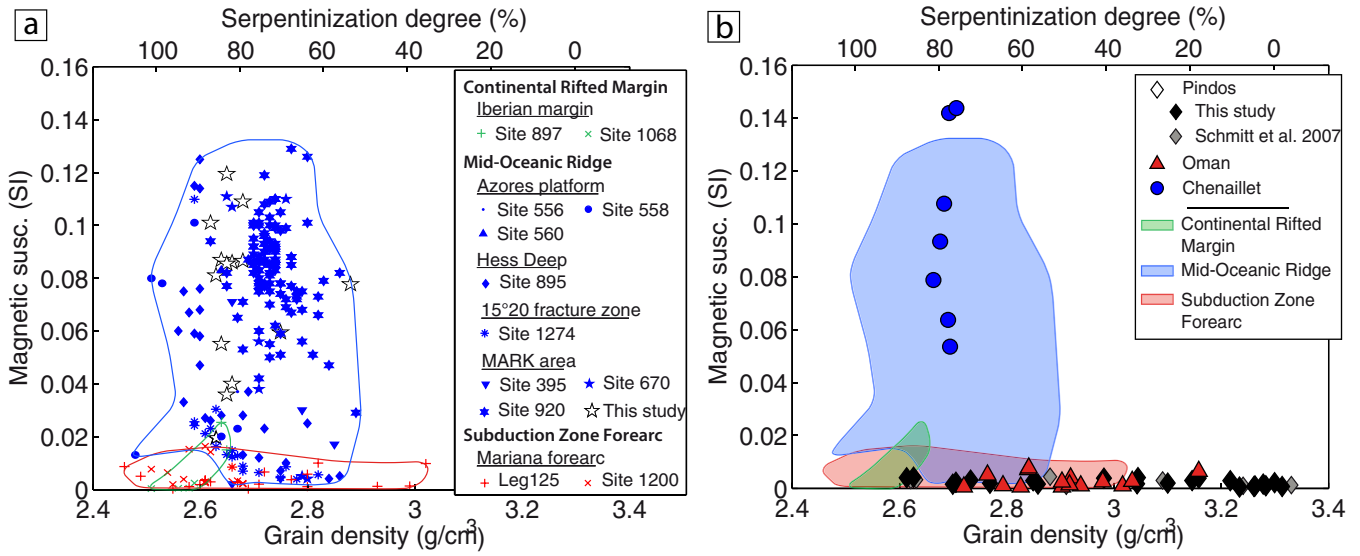

Figure 4. Susceptibility versus grain density and corresponding serpentinization degree. (a) Compilation of existing data for serpentinites from different oceanic settings. Continental rifted margins are represented by the Iberia margin (ODP sites 897 and 1068) [*Sawyer et al.*, 1994; *Zhao*, 1996; *Klein et al.*, 2014]; mid-oceanic ridges by the Azores platform (DSDP sites 556, 558 and 560) [*Bougault et al.*, 1985; *Oufi et al.*, 2002], the mid-Atlantic Ridge near Kane (DSDP site 195, ODP sites 670 and 920) [*Melson et al.*, 1978; *Detrick et al.*, 1988; *Cannat et al.*, 1995; *Oufi et al.*, 2002; *Klein et al.*, 2014], the 15°20′ Fracture Zone (IODP site 1274) [*Kelemen et al.*, 2004], and the Hess Deep (ODP site 895) [*Mével et al.*, 1993; *Oufi et al.*, 2002]; subduction zone fore arc is represented by the Mariana fore arc (ODP Leg 125 and site 1200) [*Stokking et al.*, 1992; *Salisbury et al.*, 2002; *Klein et al.*, 2014]. Our data from the MARK area are also shown (white stars). (b) Ophiolite data (this study) and distribution relative to the fields defined by the oceanic samples shown in Figure 4a. Additional data from Pindos [*Schmitt et al.*, 2007] are shown for comparison.

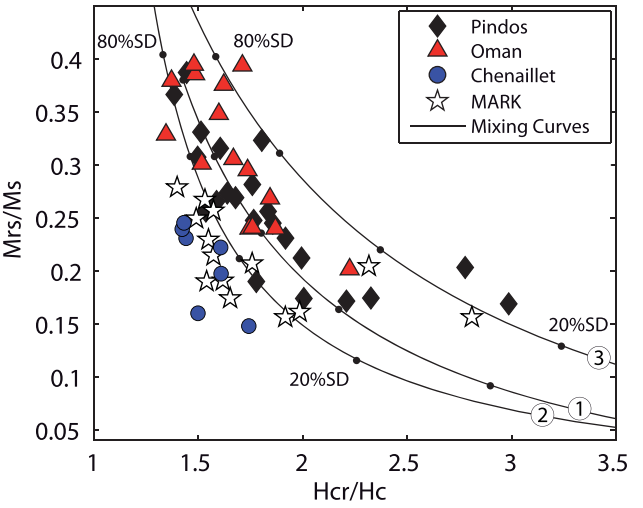

Figure 5. Domain structure of magnetite grains. Three theoretical mixing curves of single-domain and multiple-domain grains are shown in black lines. Dots are placed on the curves every 20% of SD grains content. Curves 1–3 correspond to different magnetite grain morphologies [see *Dunlop* 2002a, 2002b, for details].

brucite in the orange to brown patches locally observed on the border of serpentine-filled veins from Pindos and Oman (Figure 9b). The abundance of lizardite, and the presence of minor chrysotile and brucite, are consistent with the serpentine mineralogies classically identified in oceanic serpentinized peridotites [e.g., *Aumento and Loubat*, 1971]. The Raman data also displays a peak at 525 cm^{-1} in two of the Pindos samples (P06-2 and P13-1, Figures 9a and 9b), which may correspond to awaruite, a mineral that has already been described in serpentinites [*Lienert and Wasilewski*, 1979; *Klein and Bach*, 2009] and was spotted during SEM observations (Figures 8e and 8f). The detection of awaruite is particularly interesting for this study as awaruite has a M_s of 120 Am^2/kg, higher than that of magnetite, its contribution to bulk M_s measurement could thus be significant. However, awaruite is only spotted in a few samples with high serpentinization degree (typically above 70%) and in very small concentration as small disseminated grains (less than a few 100 nm, Figure 8f). We quantified awaruite and magnetite concentration using SEM images and element maps on samples showing the highest amounts of awaruite from the Pindos suite. Estimated awaruite content is below 0.05%, while that of magnetite is around 0.2%. We expect much lower awaruite concentration for other samples than for those selected for the quantification. Hence, awaruite does not have a significant impact on the general correlation we derived for magnetite production during serpentinization.

While there is no simple correlation between mineralogical assemblage and the degree of serpentinization, these observations show that the samples studied here can be separated in two distinct groups: first, magnetite-poor samples from the Pindos and Oman ophiolites, that contain irregular magnetite grains along serpentine veins and occasionally late brucite along vein edges, and show unaltered orthopyroxene. And second, magnetite-rich samples from the Chenaillet ophiolite and oceanic lithosphere at MARK, with euhedral magnetite crystals along mesh rims composed of lizardite, displaying orthopyroxene altered to bastite.

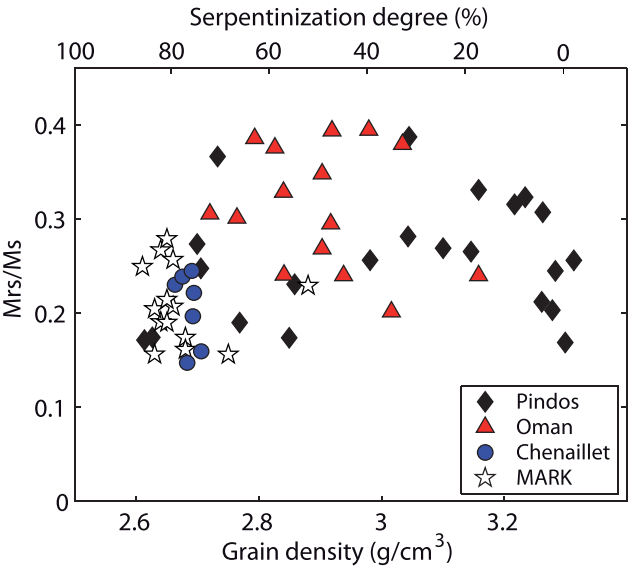

Figure 6. Evolution of the ratio M_{rs}/M_s, proxy for magnetite grain size, with grain density and corresponding serpentinization degree. The lower the M_{rs}/M_s ratio, the larger the magnetite grain sizes are.

Electron microprobe analyses of the serpentine minerals from these two groups of samples show also distinct compositions. The magnetite-poor samples (Pindos and Oman) show that serpentines from the mesh are iron-rich, with an average FeO content of ~6 wt % (supporting information Table S1) and Fe^{3+}/Fe^{Tot} ratios ranging from ~0.1 to 0.6 (supporting information Table S4). The Fe^{3+}/Fe^{Tot} of serpentine varies at the thin section scale and tends to follow

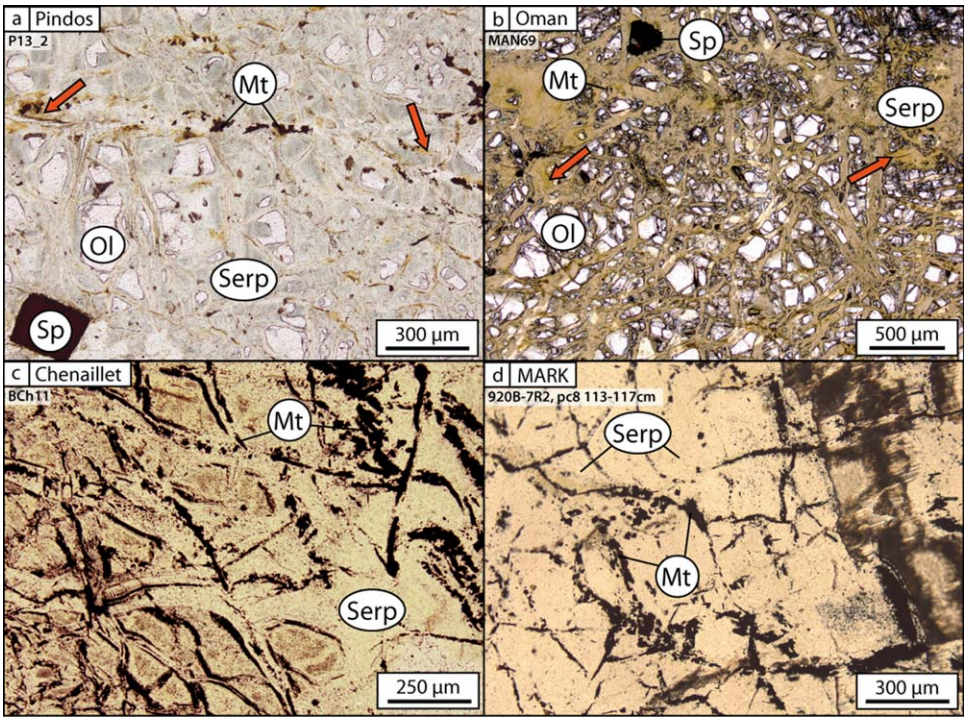

Figure 7. Photomicrographs under parallel nicols of the typical mesh texture observed in our serpentinized peridotites from (a–c) ophiolite complexes and (d) abyssal area. The mesh texture is observed in all samples. Magnetite is only found along veins for (a) Pindos and (b) Oman, whereas it is abundant in the mesh of (c) Chenaillet and (d) MARK. Orange serpentine is locally observed at Pindos and Oman and is shown with red arrows in Figures 7a and 7b. A late serpentine-filled vein is visible on the right side of the MARK photograph (Figure 7d). Mineral abbreviations: Mt, magnetite; Ol, olivine; Opx, orthopyroxene; Serp, serpentine; Sp, spinel.

the local degree of serpentinization. We also identified serpentines along late veins that have lower FeO values of ~3 wt %, but that are much less abundant. Low silica values (down to 25 wt % SiO_2) in some of the serpentine analyses may result from serpentine/brucite intergrowth [*Bach et al*., 2006]. In contrast, the magnetite-rich samples (Chenaillet and MARK) have more homogeneous serpentine composition within mesh and late veins, with low FeO values that consistently fall within the 2–4 wt % range (supporting information Table S1). These results are consistent with previous studies showing that the total iron content in serpentine is inversely correlated with modal magnetite [*Ohanley and Dyar*, 1993]. The available µXANES data of Fe^{3+}/Fe^{Tot} in serpentine minerals from MARK [*Andreani et al*., 2013] show similar ranges and trends as the one from Pindos. The FeO content of olivine in all these mantle rocks is very homogeneous, with an average Mg# around 90–92 for relic olivine grains (for Pindos see supporting information Table S2, for Oman see *Monnier et al*., [2006], for MARK see *Cannat et al*. [1995]; and *Andreani et al*. [2007]. This suggests that differences in iron content of serpentine minerals must be acquired during serpentinization, and independently from olivine composition.

To constrain the behavior of iron during serpentinization when very scarce magnetite is formed, we have studied in detail the Pindos samples suite, as it covers the widest range of serpentinization degree. Whole rock major elements analyses of these samples (supporting information Table S3) show that total iron content is relatively homogeneous, varying between ~7 and 8.5% FeO. While virtually no magnetite is formed, iron oxidation increases with increasing degree of serpentinization (Figure 10), which is consistent with the increasing amount of ferric iron measured in the Fe-rich serpentine minerals from Pindos (supporting information Table S4). Whole rock analyses of magnetite-rich MARK and Chenaillet samples (supporting information Table S3) [*Andreani et al*., 2013; *Debret et al*., 2014], which have serpentinization degrees of >50% and are shown for comparison, have heterogeneous but high values of Fe^{3+}/Fe^{Tot}, most of them being close to 0.7. It should be pointed out that they are in the same range as the Pindos samples, showing that bulk rock oxidation is not necessarily dependent on magnetite formation and can be controlled by the ferric iron integration in serpentine minerals.

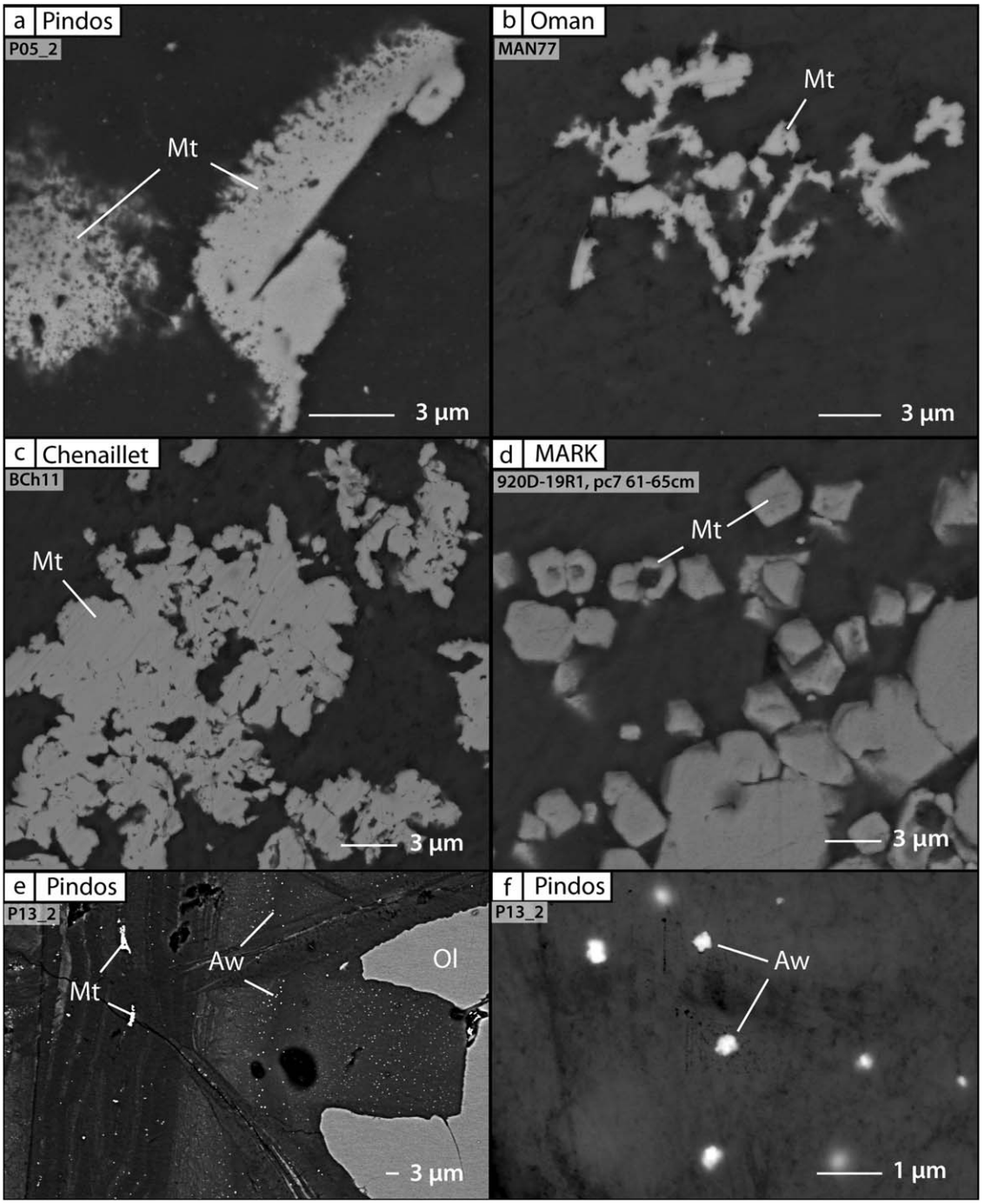

Figure 8. SEM imagery of representative magnetite grain for each of the studied ophiolites (a) Pindos, (b) Oman and (c) Chenaillet, and (d) the MARK area. (e) Awaruite (Ni_3Fe) repartition within the mesh (bright spots), and (f) a close-up of awaruite grains. Mineral abbreviations: Aw, awaruite; Ol, olivine; Mt, magnetite; Serp, serpentine.

5. Discussion

5.1. Contrasted Magnetic Properties

Previous studies from near-axis oceanic serpentinites [*Oufi et al*., 2002] and the Mirdita ophiolite [*Maffione et al*., 2014] report high magnetite content, and suggest that the amount of magnetite increases rapidly above a serpentinization degree of 60–75%, owing to the breakdown of Fe^{2+}-rich brucite [*Bach et al*., 2006] or Fe^{2+}-rich serpentine [*Andreani et al*., 2013], and to the crystallization of Fe-poor serpentine [*Oufi et al*., 2002]. In contrast, the Pindos and Oman samples, which cover the almost full range of serpentinization

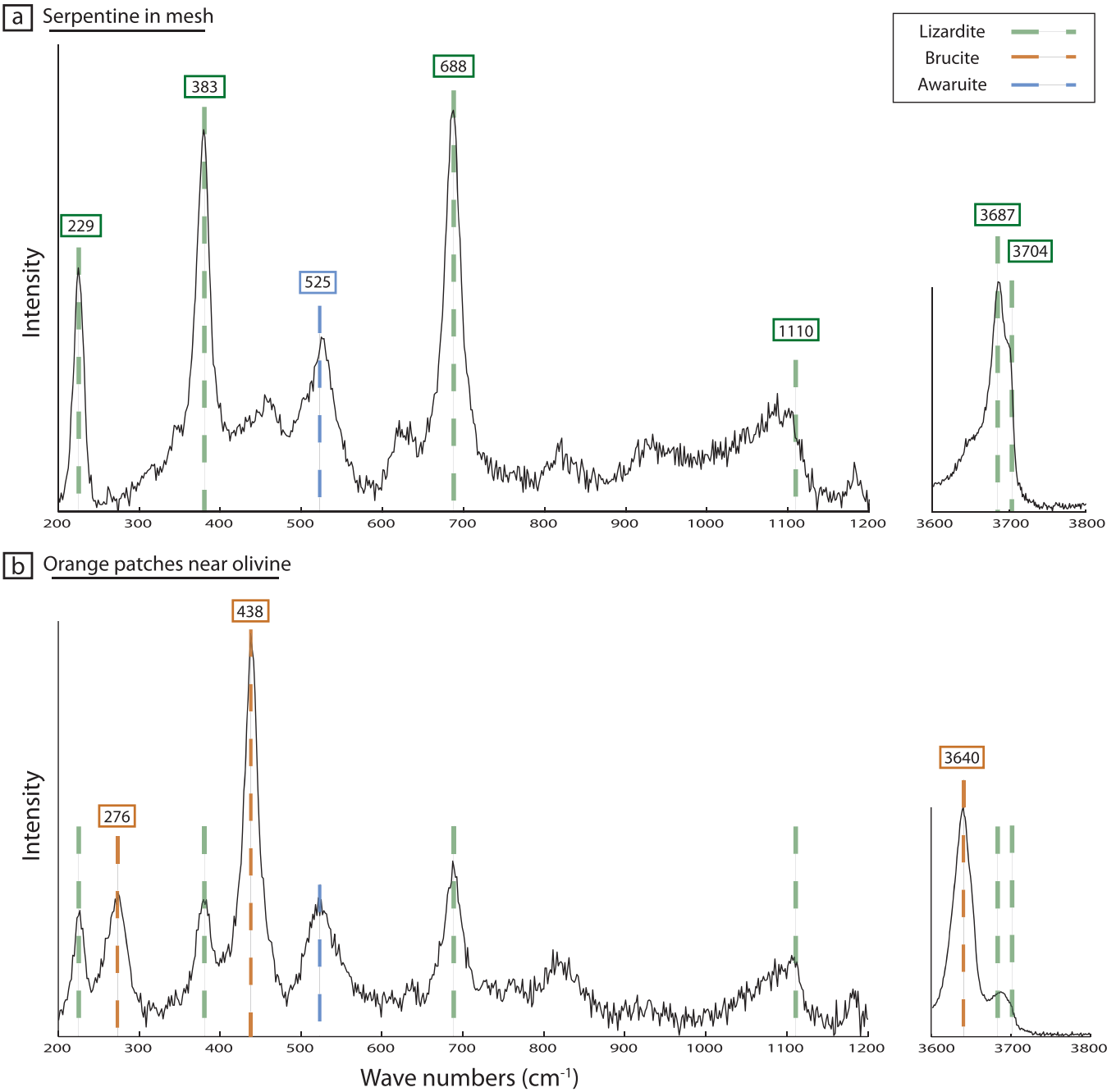

Figure 9. Representative Raman spectra of serpentine. (a) Serpentine in the mesh is almost pure lizardite (peaks indicated by the green dashed lines). (b) Orange patches observed in Pindos and Oman samples display a mixing between lizardite and brucite. Peaks observed at 525 μm are associated with awaruite. Both spectra are from Pindos sample P13-1.

degree, show a weak dependence of magnetite content and susceptibility on serpentinization degree. Above 10–15% serpentinization, we observe no increase in susceptibility with increasing serpentinization (Figure 11). The maximum amount of magnetite for these samples is less than 0.4%, and the 60 or 75% threshold for the formation of significant amounts of magnetite reported elsewhere [*Oufi et al.*, 2002; *Maffione et al.*, 2014] does not apply to the serpentinization undergone by the Pindos and Oman samples. The Chenaillet and MARK sample suites are highly serpentinized and have a narrow range of serpentinization degrees (76–81% and 57–88%, respectively), while spanning a wide range of magnetic susceptibilities and magnetite content. Considering the data scatter, it is difficult to identify a correlation with the degree of serpentinization, but high values in susceptibility and saturation remanence caused by significant amount of

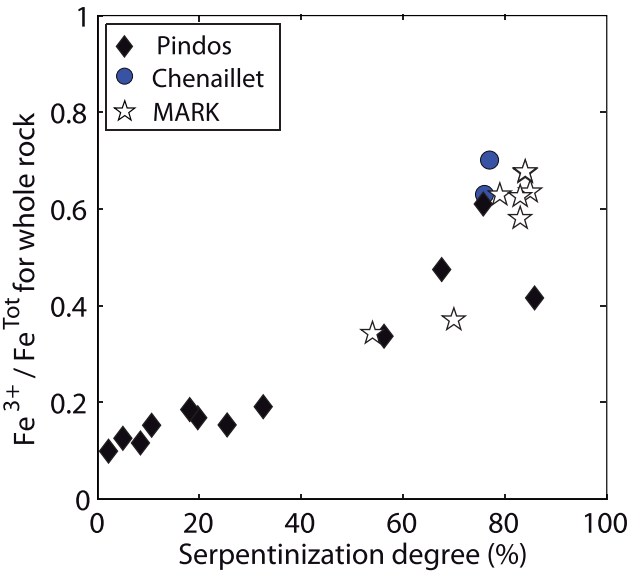

Figure 10. Fe^{3+} content in whole rock versus serpentinization degree (calculated from grain density). Data for Chenaillet are from *Debret et al*. [2014].

magnetite (up to 6.6%) are commonly observed (Figure 3). We also note that some MARK samples have low amounts of magnetite despite their high serpentinization degree (see Figures 3 and 11), but are always above the Pindos and Oman trend. Thus, Chenaillet and MARK samples, all highly serpentinized, are scattered but show a clear tendency toward high magnetite content and magnetic susceptibility.

5.2. Iron Partitioning and Oxidation State

Numerous reactions have been proposed to describe serpentinization, often seen as a multistage process. They can involve various proportion of olivine and pyroxene, possible production of brucite or silica enrichment, among other processes. To understand the magnetic consequences of serpentinization, the most important characteristics is the fate of iron initially contained in olivine ± orthopyroxene, and distributed subsequently between brucite, magnetite and serpentine. Two end-member cases have been described [*Toft et al*., 1990; *Evans et al*., 2009; *Klein et al*., 2014]. In the first case, the iron contained in silicate enters secondary serpentine minerals and/or brucite with no production of magnetite. This reaction corresponds for our samples to the following equation of olivine hydration (Fo_{90}) to form lizardite (Lz) and brucite (Br), with subscripts being mol % of Mg end-member solid solution series, after *Toft et al*. [1990] (reaction 21), (curve A in Figure 11):

$$30\,Fo_{90} + 45.00\,H_2O = 15\,Lz_{90} + 15.00\,Br_{90}.$$

In the second case, the iron contained in primary silicate phases is oxidized by water and produces hydrogen (H_2) and magnetite (Mt), with an increase of magnetic susceptibility (reaction 15 from *Toft et al*. [1990], curve B in Figure 11):

$$30\,Fo_{90} + 41.00\,H_2O = 15\,Lz + 2\,Mt + 9\,Br + 2\,H_2.$$

Toft et al. [1990] modeled the evolution of density and magnetic susceptibility with increasing degree of serpentinization, depending on the abundance of magnetite produced. Susceptibility is thus directly proportional to the magnetite produced during the course of the reaction, and the crystallization of Fe-rich serpentine and/or brucite would prevent the magnetite production, limiting susceptibility and saturation magnetization values.

The susceptibility of the Chenaillet and MARK samples (Figure 11) suggests that in these samples the iron is largely within the magnetite minerals, and thus that serpentinization is controlled by the second reaction (curve B in Figure 11). No brucite has been identified for both sites, which is consistent with observations from *Schwartz et al*. [2013] for Chenaillet and from *Oufi et al*. [2002] and *Andreani et al*. [2007] for MARK. *Dilek et al*. [1997] reported the presence of possible brucite in some samples from MARK based on anomalously low SiO_2 content in serpentine. Brucite might be present in MARK site but remains a minor phase, likely due to the availability of silica resulting from the destabilization of orthopyroxenes [e.g., *Andreani et al*., 2007].

The Pindos and Oman samples are spread over a broad area in Figure 11, but always toward low susceptibilities even at high degrees of serpentinization. In these samples iron must be incorporated in phases other than magnetite, suggesting a serpentinization consistent with the first reaction (curve A in Figure 11). In this first reaction, the iron released from iron-bearing olivine is accommodated in serpentine and brucite. The Pindos and Oman samples show serpentine minerals (and minor brucite) with high FeO content (up to

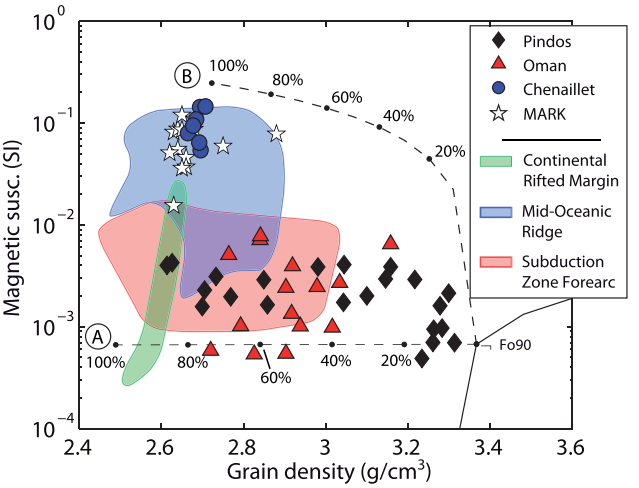

Figure 11. Susceptibility evolution according to the iron partitioning during reaction process. Two trend paths calculated following *Toft et al.* [1990] represent the two extreme reactions with no magnetite (curve A) and magnetite formation (curve B). Serpentinization degree increments of 20% are indicated along the curves by black dots and labelled. The shaded areas correspond to the three fields of oceanic serpentinites defined in Figure 4a.

~7%), confirming that serpentine is the major sink for iron (Figure 12). By contrast, Chenaillet and MARK samples show serpentine minerals with an overall lower FeO content (~2–4%) (Figure 12), compositions consistent with those observed in other mid-ocean ridge samples [*Oufi et al.*, 2002]. This suggests that the deficit in magnetite in magnetite-poor samples is compensated by iron enrichment of serpentine ± brucite minerals.

Serpentinization has been shown to release hydrogen due to the reduction of water and oxidation of ferrous iron, resulting in the production of magnetite [e.g., *Neal and Stanger*, 1983; *Charlou and Donval*, 1993; *Berndt et al.*, 1996]. The iron redox state measured in the Pindos samples (Figure 10), where little magnetite is formed, shows that most of the iron entering serpentine minerals is in the form of Fe^{3+}. Therefore, even if no magnetite is formed the oxidation of iron proceeds during the serpentinization reaction. Our observations are in agreement with prior studies suggesting that part of the hydrogen generated by serpentinization results from the oxidation of iron entering serpentine minerals [*Evans et al.*, 2009; *Andreani et al.*, 2013; *Klein et al.*, 2014]. This H_2 generation hence induces reducing conditions, consistent with the presence of native metals such as awaruite (Ni_3Fe, Figures 7e and 7f). The counter-intuitive observation of iron reduction by H_2 release due to iron oxidation has been put forward in several prior studies [e.g., *Nickel*, 1959; *Dick*, 1974; *Lienert and Wasilewski*, 1979; *Bina and Henry*, 1990]. The formation of Ni-Fe-alloys such as awaruite has been already observed in oceanic serpentinites where it coexists with magnetite but is only predicted under highly reducing conditions in low sulfur fugacity and low water-to-rock ratio environments [*Frost*, 1985; *McCollom and Bach*, 2009; *Klein and Bach*, 2009]. The corresponding concentrations of hydrogen reached for a given temperature remains difficult to predict because of the lack of thermodynamic data on metal alloys but available calculations show that awaruite can form under a large range of temperatures, as the minimum H_2 activity required is lower at $T < 250°C$ than at higher temperatures [*Klein and Bach*, 2009]. In any case, the occurrence of awaruite in Pindos samples testifies of the important H_2 production during serpentinization, creating reducing conditions similar to those observed near the serpentinization front in oceanic setting [*Alt and Shanks*, 1998]. The good preservation of awaruite in Pindos also suggests limited fluid rock-reactions after the main serpentinization stage.

5.3. Conditions of Serpentinization

Serpentinization may occur under a wide range of temperatures. We have no direct evidence for the temperature of serpentinization undergone by our sample suites (e.g., oxygen isotope fractionation), except for MARK, where IODP site 920 shows a main serpentinization event at an elevated temperature of at least 350°C [*Agrinier and Cannat*, 1997]. Our magnetic results, together with the composition of serpentinites and the petrology of samples, can provide constraints on the serpentinization processes operating at different sites. The presence of fresh orthopyroxene together with completely serpentinized olivine in Pindos and Oman samples shows that olivine hydration is the main reaction occurring during serpentinization. The main stage of serpentinization must have occurred at temperatures under which olivine reacts significantly faster than orthopyroxene, pointing to temperatures below 300°C [*Martin and Fyfe*, 1970; *Allen and Seyfried*, 2003]. In contrast, orthopyroxene in the Chenaillet and MARK samples is largely altered to bastite, suggesting serpentinization at higher temperatures, in the range of 300–400°C, and in agreement with serpentinization temperatures estimated from oxygen isotope fractionation at MARK [*Agrinier and Cannat*, 1997]. Another concordant observation is the absence of brucite in Chenaillet and MARK samples. The high silica

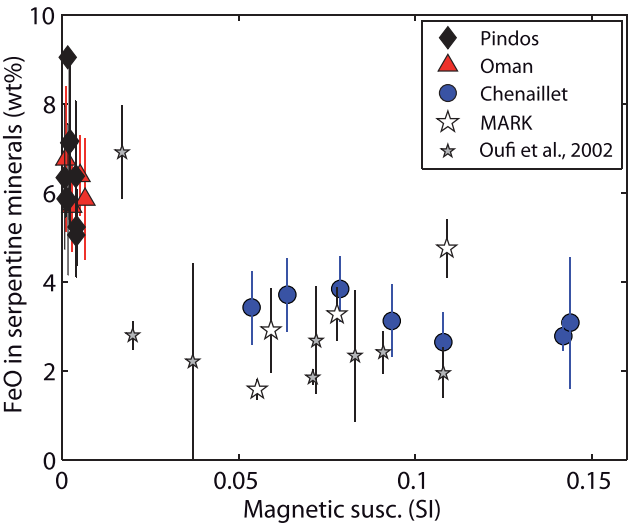

Figure 12. FeO content in serpentine minerals from mesh versus magnetic susceptibility. Analyses from MARK samples from *Oufi et al.* [2002] are shown for comparison.

activity of fluids reacting with pyroxene causes either the absence of brucite or its destabilization to serpentine with the addition of magnetite in the case of high Fe-brucite [*Bach et al.*, 2006]. An additional indication is the irreversibility of most thermomagnetic curves from Pindos and Oman samples, with crystallization of magnetite during the experiment and destabilization of Cr-spinel, suggesting the initiation of new reactions upon heating in these samples.

It has been shown by hydrothermal laboratory experiments on olivine and by thermochemical models [*Seyfried et al.*, 2007; *Evans*, 2008; *Klein et al.*, 2009; *Malvoisin et al.*, 2012a, 2012b] that if serpentinization proceeds at low temperatures (less than ~200°C), magnetite formation is limited, and iron in the ferrous and ferric form enter serpentine, forming iron-rich serpentine crystals. If serpentinization happens at higher temperature magnetite is produced along with serpentine, which adjusts its composition to a less iron-rich composition. This has been confirmed in a recent compilation of serpentinites from oceanic environments [*Klein et al.*, 2014] showing that magnetite is widespread in mid-ocean ridge settings, where serpentinization temperature (inferred from oxygen isotopes) is high (above 200–300°C), while it is scarce in margin and subduction fore-arc environments where serpentinization temperature is low (<~200°C). The high initial temperature of serpentinization at mid-ocean ridges environments may be attributed to elevated thermal gradients in the lithosphere (e.g., young crustal age, the presence of magma, among others). These thermal gradients are expected to be lower at colder margins, resulting in environments where serpentinization occurs at a lower temperature than at mid-ocean ridges.

Our study shows that Pindos and Oman samples have magnetic and petrological properties compatible with low temperature serpentinization (<~200°C) while Chenaillet and MARK samples are compatible with higher serpentinization temperatures (200–350°C). Samples collected from mid-ocean ridges, however, are characterized by heterogeneity both in their magnetic properties and the iron content of serpentine minerals. This is best explained by a long and complex serpentinization history, as observed in other sample suites [e.g., *Oufi et al.*, 2002; *Bach et al.*, 2006; *Andreani et al.*, 2007, 2013].

Based on the study of three ophiolite massifs, we suggest that serpentinization of mantle rocks from ophiolite complexes may occur under different thermal regimes, partially reflecting and controlled by the original oceanic lithosphere architecture. Both at the Pindos and Oman ophiolites the mantle was overlain by a layered, magmatic crust with a thick dyke complex, that was likely continuous laterally, and that has been well preserved during obduction in the case of Oman. This layered crust is formed along mid-ocean ridge sections with significant magma supply, and with the presence of axial magma chambers that are laterally continuous. In this context, water penetration to the mantle deep below the seafloor is expected to be limited, precluding extensive upper mantle serpentinization on axis. This is consistent with the seismic studies along fast-spreading mid-ocean ridges where the upper mantle near-axis shows seismic velocities incompatible with extensive serpentinization [e.g., *White et al.*, 1992; *Dunn et al.*, 2000]. More likely, serpentinization occurred at a later time (well off axis), with significant cooling of the lithosphere, and most probably associated with the obduction process.

In contrast, geological studies suggest that the Chenaillet ophiolite was formed at a spreading axis dominated by tectonic activity, with a heterogeneous lithosphere and a discontinuous crust allowing for peridotite outcrops at the seafloor and near-axis [*Lagabrielle and Cannat*, 1990; *Manatschal et al.*, 2011]. This type of lithosphere, which is widespread along slow to ultraslow spreading ridges [e.g., *Cannat*, 1993], is also dominated by extensive faulting, that facilitates both the tectonic uplift of deep-seated rocks to shallow levels

and the penetration of seawater into the shallow lithosphere. Mantle rocks within this lithosphere are thus serpentinized on axis, as demonstrated by the sampling of serpentinites along this type of mid-ocean ridges. In all cases, these serpentinites show evidence for high temperature serpentinization, even if recrystallization events may occur during their long tectonic history. We thus suggest that the serpentinization recorded at the Chenaillet ophiolite may have started at the axis and under a still hot thermal regime. This setting would explain the magnetic and petrological properties of the Chenaillet samples, which are very similar to mid-ocean ridge samples, and contrasting with those from Pindos and Oman. The heterogeneity in magnetic properties, consistent with what is observed at present day mid-ocean ridges (Figures 3, 11 and 12), may result from late processes of recrystallization occurring as the lithosphere cools down at the axis during the exposure or during later processes.

6. Conclusion

Our study of serpentinites from different ophiolite complexes demonstrates that they display contrasting magnetic properties that reflect their mineral assemblages and are dependent on their temperature of serpentinization. In Pindos and Oman samples, very little magnetite is produced during serpentinization, while serpentine minerals are iron rich. These samples are characterized by low magnetic susceptibility (K) and saturation magnetization (M_s). This magnetic behavior is consistent with serpentinization occurring at low temperature (below ~200°C). We suggest that in these ophiolites, characterized by a layered crust overlying the mantle reflecting high magma production and hot thermal regime, serpentinization did not occur on axis or near-axis because seawater could not penetrate into the subcrustal mantle in the absence of deep faulting. Serpentinization must thus occur well off axis, with a significantly cooler thermal regime, and most likely during the obduction processes. In Chenaillet ophiolite samples, where abundant magnetite is produced during serpentinization, the magnetic susceptibility and saturation magnetization are generally high although variable. This magnetic behavior is consistent instead with serpentinization occurring at high temperatures, likely in the 200–350°C range. We suggest that in this ophiolite, characterized by a heterogeneous lithosphere and discontinuous crust, serpentinization started at the axis because tectonic activity allowed seawater to penetrate into the mantle. The long and complex tectonic history may have resulted in recrystallization, explaining the more heterogeneous magnetic properties. Based on the two magnetically distinct sets of ophiolite serpentinites, we propose that magnetic properties can be used as a proxy to distinguish between serpentinization taking place at high temperature (near the ridge axis) and at low temperature serpentinization (occurring off axis, likely during obduction). Moreover, we also demonstrate that hydrogen is produced in both cases as the iron gets oxidized whether it enters serpentine minerals (at low serpentinization temperature) or magnetite (at high serpentinization temperature).

Acknowledgments
The authors thank C. Monnier for kindly providing the Oman samples, D. Deldicque and S. Borensztajn for helping us with the SEM analyses, M. Munoz for his help during XANES data acquisition and processing on ID24 beamline, and H. Horen for fruitful discussions. This paper also benefitted from discussions with S. Rouméjon and M. Cannat at its early stages. We thank P. Selkin and one anonymous reviewer for thoughtful comments. Parts of this work were conducted using the IPGP platform PARI, supported by Region Île-de-France SESAME grant 12015908. Analytical and sampling work were partly supported by the SYSTER program of CNRS-INSU. Supporting data are included as a Table 1 and four tables in a supporting information file. This is IPGP contribution 3752.

References

Agrinier, P., and M. Cannat (1997), Oxygen-isotope constraints on serpentinization processes in ultramafic rocks from the mid-Atlantic ridge (23°N), in *Proceedings of the Ocean Drilling Program, Scientific Results*, vol. 153, edited by J. A. Karson et al., pp. 381–388, Ocean Drill. Program, College Station, Tex., doi:10.2973/odp.proc.sr.153.033.1997.

Allen, D. E., and W. E. Seyfried (2003), Compositional controls on vent fluids from ultramafic-hosted hydrothermal systems at mid-ocean ridges: An experimental study at 400°C, 500 bars, *Geochem. Cosmochim. Acta*, *67*, 1531–1542, doi:10.1016/S0016-7037(02)01173-0.

Alt, J. C., and W. C. Shanks (1998), Sulfur in serpentinized oceanic peridotites: Serpentinization processes and microbial sulfate reduction, *J. Geophys. Res.*, *103*, 9917–9929.

Andreani, M., C. Mével, A.-M. Boullier, and J. Escartín (2007), Dynamic control on serpentine crystallization in veins: Constraints on hydration processes in oceanic peridotites, *Geochem. Geophys. Geosyst.*, *8*, Q02012, doi:10.1029/2006GC001373.

Andreani, M., M. Muñoz, C. Marcaillou, and A. Delacour (2013), μXANES study of iron redox state in serpentine during oceanic serpentinization, *Lithos*, *178*, 70–83, doi:10.1016/j.lithos.2013.04.008.

Aumento, F., and H. Loubat (1971), The mid-Atlantic ridge near 45°N. XVI. Serpentinized ultramafic intrusions, *Can. J. Earth Sci.*, *8*, 631–663, doi:10.1139/e71-062.

Bach, W., H. Paulick, C. J. Garrido, B. Ildefonse, W. P. Meurer, and S. E. Humphis (2006), Unraveling the sequence of serpentinization reactions: Petrography, mineral chemistry, and petrophysics of serpentinites from MAR 15°N (ODP Leg 209, site 1274), *Geophys. Res. Lett.*, *33*, L13306, doi:10.1029/2006GL025681.

Berndt, M. E., D. E. Allen, and W. E. Seyfried (1996), Reduction of CO_2 during serpentinization of olivine at 300°C and 500 bar, *Geology*, *24*, 351–354, doi:10.1130/0091-7613(1996)024<0351:ROCDSO>2.3.CO;2.

Bina, M. M., and B. Henry (1990), Magnetic properties, opaque mineralogy and magnetic anisotropies of serpentinized peridotites from ODP Hole 670A near the mid-Atlantic ridge, *Phys. Earth Planet. Inter.*, *65*, 88–103, doi:10.1016/0031-9201(90)90078-C.

Bougault, H., et al. (1985), *Initial Reports of the Deep Sea Drilling Project*, vol. 82, U.S. Govt. Print. Off., Wash.

Brachfeld, S. A., S. K. Banerjee, Y. Guyodo, and G. D. Acton (2002), A 13200-year history of century to millennial-scale paleoenvironmental change magnetically recorded in the Palmer Deep, western Antarctic Peninsula, *Earth Planet. Sci. Lett.*, *194*, 311–326, doi:10.1016/S0012-821X(01)00567-2.

Cannat, M. (1993), Emplacement of mantle rocks in the seafloor at mid-ocean ridges, *J. Geophys. Res.*, *98*, 4163–4172, doi:10.1029/92JB02221.

Cannat, M., et al. (1995), Proceeding of the Ocean Drilling Program, Initial Reports, vol. 153, 798 pp., Ocean Drill. Program, College Station, Tex.

Charlou, J.-L., and J.-P. Donval (1993), Hydrothermal methane venting between 12°N and 26°N along the mid-Atlantic ridge, *J. Geophys. Res.*, *98*, 9625–9642, doi:10.1029/92JB02047.

Christensen, N. I. (1978), Ophiolites, seismic velocities and oceanic crustal structure, *Tectonophysics*, *47*, 131–157, doi:10.1016/0040-1951(78)90155-5.

Christensen, N. I., and J. D. Smewing (1981), Geology and seismic structure of the Northern section of the Oman ophiolite, *J. Geophys. Res.*, *86*, 2545–2555, doi:10.1029/JB086iB04p02545.

Debret, B., M. Andreani, M. Muñoz, N. Bolfan-Casanova, J. Carlut, C. Nicollet, S. Schwartz, and N. Trcera (2014), Evolution of Fe redox state in serpentine during subduction, *Earth Planet. Sci. Lett.*, *400*, 206–218, doi:10.1016/j.epsl.2014.05.038.

Detrick, R., et al. (1988), *Proceedings of the Ocean Drilling Program, Initial Reports*, vol. 106/109, pp. 291–295, Ocean Drill. Program, College Station, Tex.

Dick, H. J. B. (1974), Terrestrial nickel-iron from the Josephine peridotite, its geologic occurrence, associations, and origin, *Earth Planet. Sci. Lett.*, *24*, 291–198, doi:10.1016/0012-821X(74)90107-1.

Dilek, Y., A. Coulton, and S. D. Hurst (1997), Serpentinization and hydrothermal veining in peridotites at site 920 in the MARK area, in *Proceedings of the Ocean Drilling Program, Scientific Results*, vol. 153, edited by J. A. Karson et al., pp. 381–388, Ocean Drill. Program, College Station, Tex.

Dullien, F. A. L. (1992), *Porous Media: Fluid Transport and Pore Structure*, 574 pp., Academic, Cambridge, Mass., doi:10.1002/aic.690380819.

Dunlop, D. J. (2002a), Theory and application of the Day plot (M_{rs}/M_s versus H_{cr}/H_c) 1. Theoretical curves and tests using titanomagnetite data, *J. Geophys. Res.*, *107*(B3), doi:10.1029/2001JB000486.

Dunlop, D. J. (2002b), Theory and application of the Day plot (M_{rs}/M_s versus H_{cr}/H_c) 2. Application to data for rocks, sediments, and soils, *J. Geophys. Res.*, *107*(B3), doi:10.1029/2001JB000487.

Dunn, R. A., D. R. Toomey, and S. C. Solomon (2000), Three-dimensional seismic structure and physical properties of the crust and shallow mantle beneath the East Pacific Rise at 9°30′N, *J. Geophys. Res.*, *105*, 23,537–23,555, doi:10.1029/2000JB900210.

Escartín, J., G. Hirth, and B. Evans (2001), Strength of slightly serpentinized peridotites: Implications for the tectonics of oceanic lithosphere, *Geology*, *29*, 1023–1026, doi:10.1130/0091-7613(2001)029<1023:SOSSPI>2.0.CO;2.

Evans, B. W. (2008), Control of the products of serpentinization by $Fe^{2+}Mg_{-1}$ exchange potential of olivine and orthopyroxene, *J. Petrol.*, *49*, 1873–1887, doi:10.1093/petrology/egn050.

Evans, B. W., S. M. Kuehner, and A. Chopelas (2009), Magnetite-free, yellow lizardite serpentinization of olivine websterite, Canyon Mountain complex, N.E. Oregon, *Am. Mineral.*, *94*, 1731–1734, doi:10.2138/am.2009.3301.

Frost, B. R. (1985), On the stability of sulfides, oxides, and native metals in serpentinites, *J. Petrol.*, *26*, 31–63.

Früh-Green, G. L., J. A. D. Connolly, and A. Plas (2004), Serpentinization of oceanic peridotites: Implications for geochemical cycles and biological activity. The subseafloor biosphere at mid-ocean ridges, *Geophys. Monogr. Ser.*, *144*, 119–135, doi:10.1029/144GM08.

Horen, H., M. Soubrand, J. Kierczak, E. Joussein, and C. Néel (2014), Magnetic characterization of ferrichromite in soils developed on serpentinites under temperate climate, *Geoderma*, *235*, 83–89, doi:10.1016/j.geoderma.2014.06.026.

Karson, J. A., et al. (1987), Along axis variations in seafloor spreading in the MARK area, *Nature*, *328*, 681–685.

Kelemen, P. B., et al. (2004), *Proceedings of the Ocean Drilling Program, Scientific Results*, vol. 209, Ocean Drill. Program, College Station, Tex., doi:10.2973/odp.proc.ir.209.2004.

Klein, F., and W. Bach (2009), Fe-Ni-Co-O-S phase relations in peridotite-seawater interactions, *J. Petrol.*, *20*, 37–59, doi:10.1093/petrology/egn071.

Klein, F., W. Bach, N. Jöns, T. McCollom, B. Moskowitz, and T. S. Berquó (2009), Iron partitioning and hydrogen generation during serpentinization of abyssal peridotites from 15°N on the Mid-Atlantic Ridge, *Geochem. Cosmochem. Acta*, *73*, 6868–6893, doi:10.1016/j.gca.2009.08.021.

Klein, F., W. Bach, and T. M. McCollom (2013), Compositional controls on hydrogen generation during serpentinization of ultramafic rocks, *Lithos*, *178*, 55–69, doi:10.1016/j.lithos.2013.03.008.

Klein, F., W. Bach, S. E. Humphris, W.-A. Kahl, N. Jöns, B. Moskowitz, and T. S. Berquó (2014), Magnetite in seafloor serpentinite—Some like it hot, *Geology*, *42*, 135–138, doi:10.1130/G35068.1.

Lagabrielle, Y., and M. Cannat (1990), Alpine Jurassic ophiolites resemble the modern central Atlantic basement, *Geology*, *18*, 319–322.

Lagabrielle, Y., and R. Polino (1988), A structural map of the ophiolite-bearing schistes lustres northwest of the Monte-Viso massif (SW Alps) and its implications, *C. R. l'Acad. Sci. Sér. II*, *306*, 921–928.

Lemoine, M., G. Boillot, and P. Tricart (1987), Ultramafic and gabbroic ocean floor of the Ligurian Tethys (Alps, Corsica, Apennines): In search of a genetic model, *Geology*, *15*, 622–625, doi:10.1130/0091-7613(1987)15<622:UAGOFO>2.0.CO;2.

Lienert, B. R., and P. J. Wasilewski (1979), A magnetic study of the serpentinization process at Burro Mountain, California, *Earth Planet. Sci. Lett.*, *43*, 406–416, doi:10.1016/0012-821X(79)90095-5.

MacLeod, C. J., J. Carlut, J. Escartín, H. Horen, and A. Morris (2011), Quantitative constraint on footwall rotations at the 15°45′N oceanic core complex, Mid-Atlantic Ridge: Implications for oceanic detachment fault processes, *Geochem. Geophys. Geosyst.*, *12*, Q0AG03, doi:10.1029/2011GC003503.

Maffione, M., A. Morris, O. Plümper, and D. J. J. van Hinsbergen (2014), Magnetic properties of variably serpentinized peridotites and their implication for the evolution of oceanic core complexes, *Geochem. Geophys. Geosyst.*, *15*, 923–944, doi:10.1002/2013GC004993.

Malvoisin, B., J. Carlut, and F. Brunet (2012a), Serpentinization of oceanic peridotites: 1. A high-sensitivity method to monitor magnetite production in hydrothermal experiments, *J. Geophys. Res.*, *117*, B01104, doi:10.1029/2011JB008612.

Malvoisin, B., F. Brunet, J. Carlut, S. Rouméjon, and M. Cannat (2012b), Serpentinization of oceanic peridotites: 2. Kinetics and processes of San Carlos olivine hydrothermal alteration, *J. Geophys. Res.*, *117*, B04102, doi:10.1029/2011JB008842.

Manatschal, G., D. Sauter, A. M. Karpoff, E. Masini, G. Mohn, Y. Lagabrielle (2011), The Chenaillet ophiolite in the French/Italian Alps: An ancient analogue for an oceanic core complex?, *Lithos*, *124*, 169–184, doi:10.1016/j.lithos.2010.10.017.

Martin, B., and W. S. Fyfe (1970), Some experimental and theoretical observations on the kinetics of hydration reactions with particular reference to serpentinization, *Chem. Geol.*, *6*, 185–202, doi:10.1016/0009-2541(70)90018-5.

McCollom, T. M., and W. Bach (2009), Thermodynamic constraints on hydrogen generation during serpentinization of ultramafic rocks, *Geochem. Cosmochem. Acta*, *73*, 856–875, doi:10.1016/j.gca.2008.10.032.

Melson, W. G., P. D. Rabinowitz, J. H. Natland, H. Bougault, and H. P. Johnson (1978), *Initial Reports of the Deep Sea Drilling Project*, vol. 45, pp. 587–594, U.S. Govt. Print. Off., Washington, D. C.

Mével, C. (2003), Serpentinization of abyssal peridotites at mid-ocean ridges, *C. R. Geosci.*, *335*, 825–852, doi:10.1016/j.crte.2003.08.006.

Mével, C., M. Cannat, P. Gente, E. Marion, J. M. Auzende, and J. A. Karson (1991), Emplacement of deep crustal and mantle rocks on the west median valley wall of the MARK area (M.A.R., 23°N), *Tectonophysics*, *190*, 31–54.

Mével, C., et al. (1993), *Proceedings of the Ocean Drilling Program, Initial Reports*, vol. 147, Ocean Drill. Program, College Station, Tex.

Miller, D. J., and N. I. Christensen (1997), Seismic velocities of lower crustal and upper mantle rocks from the slow-spreading mid-Atlantic ridge, South of the Kane Transform zone (MARK), in *Proceeding of the Ocean Drilling Program, Scientific Results*, vol. 153, edited by J. A. Karson et al., pp. 437–454, Ocean Drill. Program, College Station, Tex., doi:10.2973/odp.proc.sr.153.043.1997.

Monnier, C., J. Girardeau, and L. Le Mée (2006), Along-ridge petrological segmentation of the mantle in the Oman ophiolite, *Geochem. Geophys. Geosyst.*, *7*, Q11008, doi:10.1029/2006GC001320.

Muñoz, M., V. De Andrade, O. Vidal, E. Lewin, S. Pascarelli, and J. Susini (2006), Redox and speciation micro-mapping using dispersive X-ray absorption spectroscopy: Application to iron in chlorite mineral of a metamorphic rock thin section, *Geochem. Geophys. Geosyst.*, *7*, Q11020, doi:10.1029/2006GC001381.

Neal, C., and G. Stanger (1983), Hydrogen generation from mantle source rocks in Oman, *Earth Planet. Sci. Lett.*, *66*, 315–320, doi:10.1016/0012-821X(83)90144-9.

Nickel, E. H. (1959), The occurrence of native nickel-iron in the serpentine rock of the eastern townships of Quebec Province, *Can. Mineral.*, *6*, 307–319.

Nicolas, A., F. Boudier, and B. Ildefonse (1996), Variable crustal thickness in the Oman ophiolite: Implication for oceanic crust, *J. Geophys. Res.*, *10*, 17,941–17,950, doi:10.1029/96JB00195.

Nicolas, A., F. Boudier, and L. France (2009), Subsidence in magma chamber and the development of magmatic foliation in Oman ophiolite gabbros, *Earth Planet. Sci. Lett.*, *284*, 76–87, doi:10.1016/j.epsl.2009.04.012.

O'Reilly, W. (1984), *Rock and Mineral Magnetism*, 220 pp., Springer, U.S., doi:10.1007/978-1-4684-8468-7.

Ohanley, D. S., and M. D. Dyar (1993), The composition of lizardite 1T and the formation of magnetite in serpentines, *Am. Mineral.*, *78*, 391–404.

Oufi, O., M. Cannat, and H. Horen (2002), Magnetic properties of variably serpentinized abyssal peridotites, *J. Geophys. Res.*, *107*(B5), doi:10.1029/2001JB000549.

Rassios, A. H. E., and E. M. Moores (2006), Heterogeneous mantle complex, crustal processes, and obduction kinematics in a unified Pindos–Vourinos ophiolitic slab (northern Greece), in *Tectonic Development of the Eastern Mediterranean Region*, edited by A. H. F. Robertson and D. Mountrakis, *Geol. Soc. London, Spec. Publ.*, 260, 237–266.

Rassios, A. E., and Y. Dilek (2009), Rotational deformation in the Jurassic Mesohellenic ophiolites, Greece, and its tectonic significance, *Lithos*, *108*, 207–223, doi:10.1016/j.lithos.2008.09.005.

Robertson, A. H. F. (2002), Overview of the genesis and emplacement of Mesozoic ophiolites in the Eastern Mediterranean Tethyan region, *Lithos*, *65*, 1–67, doi:10.1016/S0024-4937(02)00160-3.

Saccani, E., and A. Photiades (2004), Mid-ocean ridge and supra-subduction affinities in the Pindos ophiolites (Greece): Implications for magma genesis in a forearc setting, *Lithos*, *73*, 229–253, doi:10.1016/j.lithos.2003.12.002.

Salisbury, M. H, et al. (2002), *Proceedings of the Ocean Drilling Program, Initial Reports*, vol. 195, Ocean Drill. Program, College Station, Tex., doi:10.2973/odp.proc.ir.195.103.2002.

Sawyer, D. S., et al. (1994), *Proceeding of the Ocean Drilling Program, Initial Reports*, vol. 149, 719 pp., Ocean Drill. Program, College Station, Tex.

Schmitt, D. R., Z. Han, V. A. Kravchinsky, and J. Escartín (2007), Seismic and magnetic anisotropy of serpentinized ophiolite: Implications for oceanic spreading rate dependent anisotropy, *Earth Planet. Sci. Lett.*, *261*, 590–601, doi:10.1016/j.epsl.2007.07.024.

Schwartz, S., S. Guillot, B. Reynard, R. Lafay, B. Debret, C. Nicollet, P. Lanari, and A. L. Auzande (2013), Pressure–temperature estimates of the lizardite/antigorite transition in high pressure serpentinites, *Lithos*, *178*, 197–210, doi:10.1016/j.lithos.2012.11.023.

Seyfried, W. E., D. I. Foustoukos, and Q. Fu (2007), Redox evolution and mass transfer during serpentinization: An experimental and theoretical study at 200°C, 500 bar with implications for ultramafic-hosted hydrothermal systems at Mid-Ocean Ridges, *Geochem. Cosmochem. Acta*, *71*, 3872–3886, doi:10.1016/j.gca.2007.05.015.

Smirnov, A. V. (2009), Grain size dependence of low-temperature remanent magnetization in natural and synthetic magnetite: Experimental study, *Earth Planets Space*, *61*, 119–124.

Stokking, L., D. Merrill, R. Haston, J. Ali, and K. Saboda (1992), Rock magnetic studies of serpentinite seamounts in the Mariana and Izu-Bonin regions, in *Proceedings of the Ocean Drilling Program, Scientific Results*, vol. 125, edited by P. Fryer et al., pp. 561–580, Ocean Drill. Program, College Station, Tex., doi:10.2973/odp.proc.sr.125.158.1992.

Toft, P. B., J. Arkani-Hamed, and S. E. Haggerty (1990), The effects of serpentinization on density and magnetic susceptibility: A petrophysical model, *Phys. Earth Planet. Inter.*, *65*, 137–157, doi:10.1016/0031-9201(90)90082-9.

Wilke, M., F. Farges, P. Petit, G. Brown, and F. Martin (2001), Oxidation state and coordination of Fe in minerals: An Fe K-XANES spectroscopic study, *Am. Mineral.*, *86*, 714–730.

White, R. S., D. McKenzie, and R. K. O'Nions (1992), Oceanic crustal thickness from seismic measurements and rare earth element inversions, *J. Geophys. Res.*, *97*, 19,683–19,715, doi:10.1029/92JB01749.

Zhao, X. (1996), Magnetic signatures of peridotite rocks from Sites 897 and 899 and their implications, in *Proceeding of the Ocean Drilling Program, Scientific Results*, vol. 149, edited by R. B. D. S. Whitmarsh Sawyer and A. D. G. Klaus Masson, pp. 431–446, Ocean Drill. Program, College Station, Tex., doi:10.2973/odp.proc.sr.149.214.1996.